

Geophysical Research Letters®



RESEARCH LETTER

10.1029/2023GL107968

Key Points:

- First observation of magnetic reconnection between magnetic flux rope (MFR) and magnetic hole (MH) in the magnetosheath
- A thin current sheet with typical reconnection signatures was formed at the interface of MFR and MH due to their interaction
- An elongated electron diffusion region was detected in the reconnection exhaust

Supporting Information:

Supporting Information may be found in the online version of this article.

Correspondence to:

R. Wang,
rswan@ustc.edu.cn

Citation:

Wang, S., Wang, R., Lu, Q., Lu, S., & Huang, K. (2024). Direct observation of magnetic reconnection resulting from interaction between magnetic flux rope and magnetic hole in the Earth's magnetosheath. *Geophysical Research Letters*, 51, e2023GL107968. <https://doi.org/10.1029/2023GL107968>






Received 20 DEC 2023

Accepted 29 APR 2024

© 2024. The Authors. Geophysical Research Letters published by Wiley Periodicals LLC on behalf of American Geophysical Union.

This is an open access article under the terms of the [Creative Commons Attribution License](https://creativecommons.org/licenses/by/4.0/), which permits use, distribution and reproduction in any medium, provided the original work is properly cited.

Direct Observation of Magnetic Reconnection Resulting From Interaction Between Magnetic Flux Rope and Magnetic Hole in the Earth's Magnetosheath

Shimou Wang^{1,2,3} , Rongsheng Wang^{1,2,3} , Quanming Lu^{1,2,3} , San Lu^{1,2,3} , and Kai Huang^{4,5} 

¹Deep Space Exploration Laboratory/School of Earth and Space Sciences, University of Science and Technology of China, Hefei, China, ²CAS Center for Excellence in Comparative Planetology/CAS Key Laboratory of Geospace Environment/Anhui Mengcheng National Geophysical Observatory, University of Science and Technology of China, Hefei, China, ³Collaborative Innovation Center of Astronautical Science and Technology, Harbin, China, ⁴School of Physics, Harbin Institute of Technology, Harbin, China, ⁵Laboratory for Space Environment and Physical Sciences, Harbin Institute of Technology, Harbin, China

Abstract We report in situ observation of magnetic reconnection between magnetic flux rope (MFR) and magnetic hole (MH) in the magnetosheath by the Magnetospheric Multiscale mission. The MFR was rooted in the magnetopause and could be generated by magnetopause reconnection therein. A thin current sheet was generated due to the interaction between MFR and MH. The sub-Alfvénic ion bulk flow and the Hall field were detected inside this thin current sheet, indicating an ongoing reconnection. An elongated electron diffusion region characterized by non-frozen-in electrons, magnetic-to-particle energy conversion, and crescent-shaped electron distribution was detected in the reconnection exhaust. The observation provides a mechanism for the dissipation of MFRs and thus opens a new perspective on the evolution of MFRs at the magnetopause. Our work also reveals one potential fate of the MHs in the magnetosheath which could reconnect with the MFRs and further merge into the magnetopause.

Plain Language Summary Magnetic flux rope (MFR) is a kind of helical magnetic field structure that is frequently observed in the Earth's magnetosphere. At the dayside magnetopause, MFRs are generally generated by the reconnection of the Earth's intrinsic magnetic field and the interplanetary magnetic field, especially when the interplanetary magnetic field points southward. These MFRs tend to grow larger after they are expelled from the reconnection sites and then travel along the magnetopause, and ultimately disintegrate into the cusp. In this study, we provide another potential fate of these magnetopause MFRs. They can interact with the magnetosheath magnetic holes and dissipate through reconnection with multiple magnetic holes. Based on the Magnetospheric Multiscale observation, we provide direct evidence of reconnection between the MFR and the magnetic hole, which has a pivotal role in this scenario. Our results give new insights into the evolution of MFRs at the magnetopause and further the coupling between the solar wind and the Earth's magnetosphere.

1. Introduction

Magnetic flux ropes (MFRs) characterized by helical magnetic field lines are ubiquitous in space plasma environments. These structures are widely considered to be generated by magnetic reconnection (Daughton et al., 2011; Drake et al., 2006; S. Lu et al., 2019) and have been observed in reconnection outflow (S. Y. Huang et al., 2019; Øieroset et al., 2016; Slavin et al., 2003; S. Wang et al., 2019) or diffusion region (Eastwood et al., 2007; Fu et al., 2017; R. Wang et al., 2010, 2016; Zhong et al., 2018). At the magnetopause, MFR is frequently termed flux transfer event (Russell & Elphic, 1978), and their structure, extension, and shape have been extensively investigated based on in situ measurements (Fear et al., 2008; Hwang et al., 2016; Owen et al., 2001; Pu et al., 2013; Zhang et al., 2012). The typical observational signature of these MFRs is a bipolar variation in the magnetic field component normal to the nominal magnetopause, usually accompanied by the enhancement of the axial component. These MFRs have diameters ranging from the microscale (ion or electron inertial length) to the macroscale (tens of Earth radii), corresponding to different generation mechanisms or temporal evolution (Eastwood et al., 2016; Fear et al., 2012; H. Hasegawa et al., 2023). Of particular interest is their ultimate fate, as it affects flux and energy transfer in the magnetosphere.

It is generally believed that MFRs can be formed in a current sheet by multiple X-line reconnection (Lee & Fu, 1985; Raeder, 2006). Previous spacecraft observations have found direct evidence of this model, that is, convective plasma flows toward the center of MFR (H. Hasegawa et al., 2010; Hwang et al., 2018; Øieroset et al., 2011). Recent observations have revealed the occurrences of ion-scale or electron-scale MFRs (Z. Chen et al., 2021; Eastwood et al., 2016; H. Hasegawa et al., 2023; Teh et al., 2017; R. S. Wang et al., 2010), which are interpreted as a result of secondary reconnection (Daughton et al., 2006; Drake et al., 2006; C. Huang et al., 2011). These secondary MFRs tend to grow larger in size after they are expelled from the reconnection X-line and travel in the exhaust region (Dong et al., 2017; H. Hasegawa et al., 2023; R. S. Wang et al., 2024). The statistical work also supports that the average size of MFRs is smaller at the subsolar magnetopause and grows as they travel toward flanks and high-latitude magnetopause (Akhavan-Tafti et al., 2018). The growth of MFR can be caused by the coalescence of two neighboring MFRs (J. Guo et al., 2021; Omid & Sibeck, 2007; R. S. Wang et al., 2017; Zhou et al., 2017) or pressure imbalance between the MFR and surrounding magnetosheath (Akhavan-Tafti et al., 2019). These growing MFRs finally achieve a quasi-equilibrium state and can be convected far downtail (Eastwood et al., 2012) or disintegrate within or tailward of the cusp (Omid & Sibeck, 2007). Another possible fate of MFRs is decay and erosion (H. Hasegawa et al., 2016), however, the mechanism by which MFRs are dissipated remains vague and lacks in situ evidence.

Mirror mode structures are often observed in the Earth's magnetosheath (Lucek et al., 2001; Tsurutani et al., 1982) and are generated by the mirror instability associated with temperature anisotropy. They are typically observed as trains of local magnetic field enhancements or depressions, accompanied by anticorrelated variation of plasma density (Soucek et al., 2008; Yao et al., 2018). They are non-propagating structures in the plasma rest frame and convected with the magnetosheath flow (Horbury et al., 2004). Laitinen et al. (2010) suggested that these magnetosheath mirror mode structures can modulate the outflow velocity of magnetopause reconnection. Based on global hybrid-Vlasov simulation, Hoilijoki et al. (2017) found that mirror mode structures can change the local plasma parameters near the reconnection X-line and thus affect the reconnection rate. These studies imply that the mirror mode structures also play a role in the dayside reconnection.

In this study, we present the first in situ observation of the interaction between MFR and magnetic hole (MH) in the magnetosheath. Magnetic reconnection occurs between MFR and MH, which leads to the dissipation of the MFR. We used the data from the Fluxgate Magnetometer (Russell et al., 2016), Electric Double Probes (Ergun et al., 2016; Lindqvist et al., 2016), and Fast Plasma Investigation (Pollock et al., 2016) of the Magnetospheric Multiscale (MMS) (Burch, Moore, et al., 2016) mission.

2. Event Overview

Figures 1a–1g show an overview of MMS1 observations from 02:50 to 03:30 UT on 15 November 2015, when the spacecraft was located at approximately $(10.2, -0.1, -0.5) R_E$ in the Geocentric Solar Ecliptic (GSE) coordinates. The average separation of the four MMS spacecraft was ~ 19 km. The ion and electron energy spectra (Figures 1a and 1b) were consistent with the features of magnetosheath plasma. During this interval, the magnetic field was fluctuating and had a significant B_y component (Figure 1c). In addition, MMS1 observed a large-scale rotation in B_z from positive to negative to positive. The general profile of magnetic field variation in the magnetosheath was almost identical to that observed in the solar wind (Figure 1h), with about 7 min delay relative to the OMNI observations, which are solar wind conditions at the nose of the bow shock. This indicates that the large-scale current sheets in the magnetosheath originated from the solar wind. The magnetic field was amplified by a factor of about 10 after crossing the bow shock.

Examining magnetic field fluctuations in the magnetosheath, we found a series of small-scale MHs in the form of dips in magnetic field strength. The B_y component showed the most significant decrease. Assuming these MHs were convected with the plasma flow, their size was approximately 400–1,800 km, ~ 10 –43 ion inertial lengths d_i based on the magnetosheath density of $\sim 29 \text{ cm}^{-3}$. Inside these MHs, plasma number density increased (Figure 1d), exhibiting an anticorrelation with magnetic field strength. Figure 1f plots the total, magnetic, electron, and ion pressures. The variation of plasma thermal pressure (sum of electron and ion pressures) was anticorrelated with the magnetic pressure, and the increased thermal pressure was compensated by a drop in magnetic pressure. Total pressure was almost constant across MHs, indicating that the structures were approximately in pressure balance. Figure 1g plots the mirror instability parameter $R = \frac{T_{\perp i}}{T_{\parallel i}} - \left(1 + \frac{1}{\beta_{\perp i}}\right)$ (A.

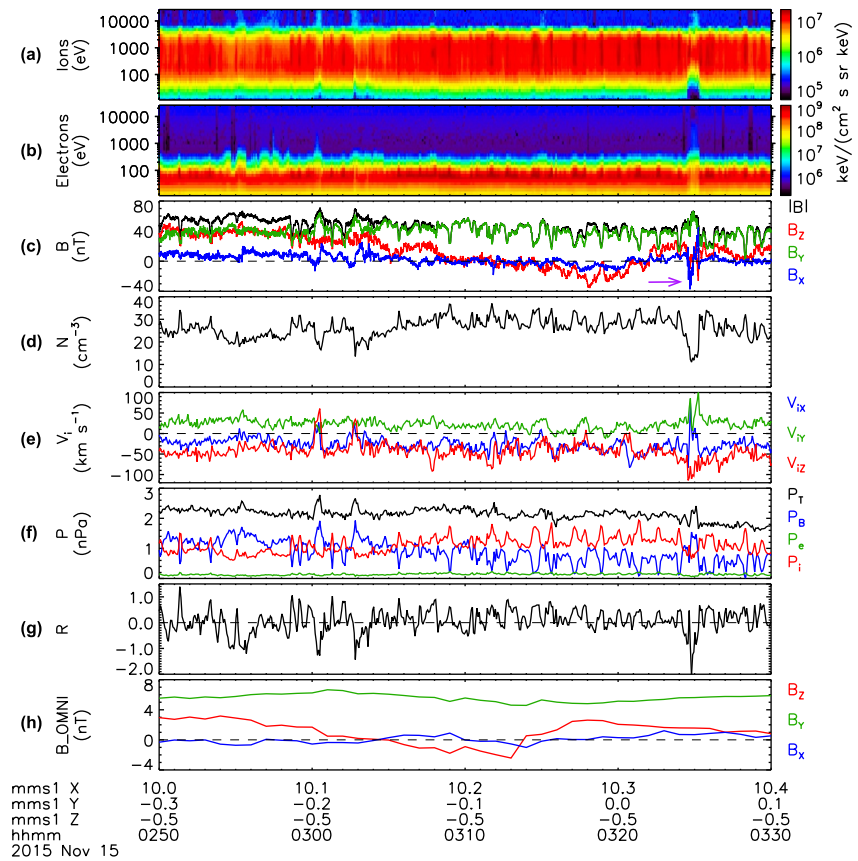


Figure 1. Overview of the event. (a)–(b) Ion and electron energy-time spectra, (c) magnetic field and its magnitude, (d) electron number density, (e) ion bulk velocity, (f) total, magnetic, electron, and ion pressures, (g) mirror instability parameter $R = \frac{T_{\perp i}}{T_{\parallel i}} - \left(1 + \frac{1}{\beta_{\perp i}}\right)$, and (h) solar wind magnetic field. The data are displayed in Geocentric Solar Ecliptic (GSE) coordinate system.

Hasegawa, 1969), with the criterion for instability development being $R > 0$. This condition was satisfied inside all the MHs. These signatures imply that the observed MHs were mirror mode structures. The criteria for linear polarization of mirror mode structures used by Soucek et al. (2008) were also checked. The analysis of eigenvalue ratios from the minimum variance analysis (MVA) of the magnetic field (Sonnerup & Scheible, 1998) shows that approximately 55% of MHs were linearly polarized and the others were elliptically polarized. The result that not all the mirror modes were linearly polarized is consistent with previous studies (Génot et al., 2001). We also examined the 3-s cadence Wind satellite data (Figure S1 in Supporting Information S1) and found these MHs were not present upstream of the bow shock, which further suggests that they were generated locally in the magnetosheath, not from the solar wind.

Except for the MHs, MMS1 observed three MFRs with increased magnetic field strength, located at $\sim 03:00:30$, $\sim 03:02:50$, and $\sim 03:25:00$ UT respectively. Each of these MFRs is characterized by a bipolar B_x signature from negative to positive accompanied by a peak of B_y around its center. Another typical feature of MFR is that the total pressure peaked at the center of all three MFRs, generating a pressure force pointing radially outward from the center. The mixture of high-energy plasma from the magnetosphere and low-energy plasma from the magnetosheath inside these MFRs indicates that they were generated by magnetopause reconnection. Especially, the third MFR was probably generated when the magnetosheath B_z was southward between 03:15 and 03:21 UT. The ion flows associated with these MFRs showed large changes in directions and magnitudes (Figure 1e). These three MFRs were all surrounded by numerous MHs, and we will focus on the MFR at $\sim 03:25:00$ UT (purple arrow in Figure 1c) in the following, which was observed to interact with the MH.

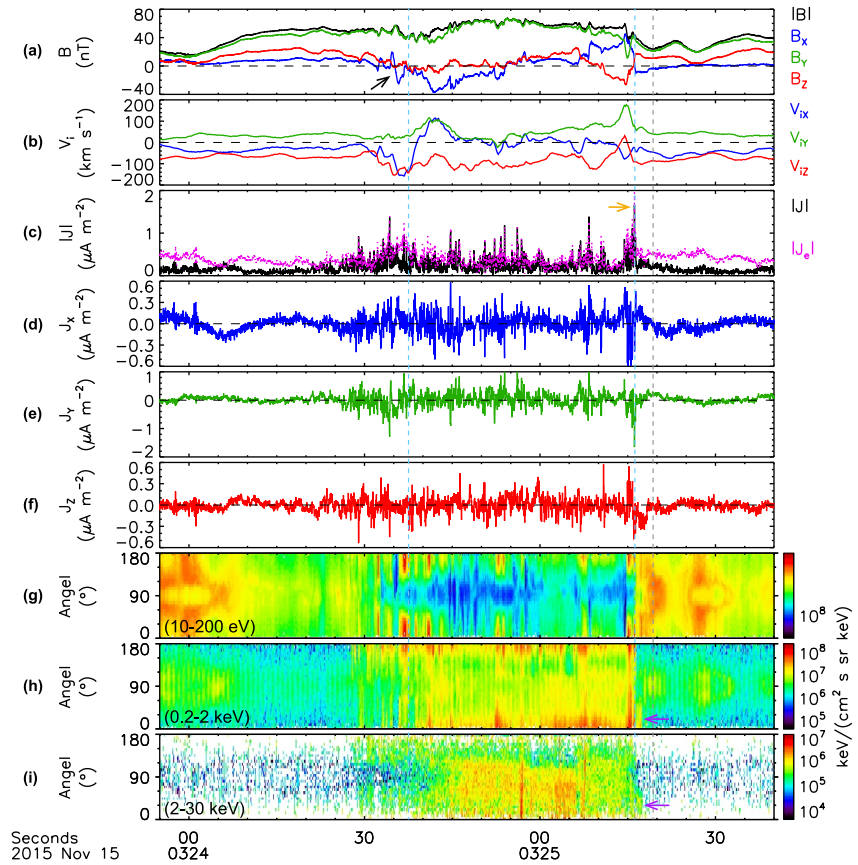


Figure 2. Details of magnetic flux rope and magnetic holes around it. (a) Magnetic field and its magnitude, (b) ion bulk velocity, (c) total and electron current density, (d)–(f) three components of current density, and (g)–(i) pitch angle distributions of low-energy (10–200 eV), mid-energy (0.2–2 keV), and high-energy (2–30 keV) electrons.

3. Interaction Between MFR and MH

Figure 2 shows a zoomed-in view of MFR and MHs around it. The rotation of B_x from negative to positive corresponding to the MFR was evident (Figure 2a). The four-spacecraft timing method (Schwartz, 1998) is performed to the B_x reversal point, and the propagation speed is calculated to be 84.5 km/s along $(0.33, 0.08, -0.94)_{\text{GSE}}$. Thus, the thickness of the MFR is estimated to be 3,380 km, $\sim 80.5 d_i$. The MFR boundaries are marked by vertical blue dashed lines based on the B_x profile. A much smaller-scale bipolar B_x variation from positive to negative (black arrow in Figure 2a) was observed near the leading edge of the MFR. This signature was observed by four spacecraft and may represent another small-scale MFR or the periphery of a MFR. The trailing edge of the MFR was bounded by a MH, with the center indicated by a vertical gray dashed line. The leading part of the MH was moving at 71.5 km/s along $(-0.24, 0.35, -0.90)_{\text{GSE}}$ according to the timing method and had a width of 465 km, $\sim 11.2 d_i$. The depth of this MH $\Delta B/B$ was ~ 0.3 .

The interaction between MFR and MH can be seen from the sharp rotation of B_x and B_z at $\sim 03:25:15$ UT, differing from the gradual variation of B_x at the leading edge at $\sim 03:24:40$ UT. A thin current sheet, corresponding to the sharp change of magnetic field, is expected at the interface of MFR and MH. A sketch of the spacecraft trajectory through MFR, MH, and the current sheet between them is shown in Figure 4a. We found that B_x and B_z increased in magnitude on approach to the current sheet center from both sides. It could be caused by the magnetic field pileup as a result of compression. The B_y and $|B|$ showed a significant drop just before the second vertical blue dashed line inside this interface current sheet, suggesting magnetic energy dissipation therein.

Figure 2c plots the total and electron current density intensities. Here, the current density is calculated from $\mathbf{J} = N_e e (\mathbf{V}_i - \mathbf{V}_e)$ where N_e is the electron number density (assuming a quasi-neutral proton plasma), e is the elementary charge, and \mathbf{V}_i and \mathbf{V}_e are the ion and electron bulk velocities. The electron current density is calculated from

$\mathbf{J}_e = -N_e e \mathbf{V}_e$. Many well-separated current spikes, that is, the filamentary currents (Eastwood et al., 2016; S. M. Wang et al., 2020, 2023), were observed inside the MFR. The current density was strong, larger than $1 \mu\text{A}/\text{m}^2$ in some filamentary currents that were mainly supplied by the electron currents. Figures 2d–2f plot three components of \mathbf{J} , respectively. Inside the MFR, currents in all three directions showed isolated spikes. The J_y component, which was roughly along the MFR axis, was stronger than J_x and J_z . Especially, some negative J_y spikes, for example, at $\sim 03:24:45$ and $\sim 03:24:52$ UT, and some positive J_y spikes, for example, at $\sim 03:24:57$ and $\sim 03:25:08$ UT, corresponded to the visible small-scale fluctuations of the magnetic fields in Figure 2a, which may reveal localized distortion or twist of magnetic field lines inside the MFR (C. Huang et al., 2017; Q. M. Lu et al., 2023).

The current density $|\mathbf{J}|$ inside the MH at $\sim 03:25:20$ UT was weak, but slightly larger than those inside other MHs, for example, at $\sim 03:24:00$ (a complete crossing of this MH was not covered by burst-mode data) and $\sim 03:25:27$ UT. The increase of $|\mathbf{J}|$ inside this MH was mainly due to the interaction between MFR and MH, since $|\mathbf{J}|$ was more significant closer to the trailing edge of the MFR. At the interface current sheet between MFR and MH, a large current spike up to $1.6 \mu\text{A}/\text{m}^2$ (orange arrow in Figure 2c) was detected. This current was dominated by $-J_y$, contrary to the primarily positive J_y inside the MFR.

Figures 2g–2i present pitch angle distributions of low-energy (10–200 eV), mid-energy (0.2–2 keV), and high-energy (2–30 keV) electrons. For the MFR, electron pitch angle distributions were energy-dependent. The low-energy and mid-energy electrons were mostly counter-streaming, while the high-energy electrons were concentrated in 0° – 90° pitch angles, suggesting an open magnetic field topology connecting the southern magnetosphere to the magnetosheath (Fear et al., 2007; Pu et al., 2013). This open field line geometry allows the escape of magnetosphere energetic electrons into the magnetosheath. For the MH at $\sim 03:25:20$ UT, electron fluxes peaked in the direction perpendicular to the magnetic field (Figures 2g and 2h). In contrast, pitch angle spectra in the MH at $\sim 03:25:27$ UT showed the donut shape (J. H. Li et al., 2021; Yao et al., 2018). Note that there were almost no high-energy electrons inside the MHs at $\sim 03:24:00$ UT and $\sim 03:25:27$ UT (Figure 2i), which suggests that their field lines were not connected to the magnetosphere. For the MH at $\sim 03:25:20$ UT, however, MMS observed visible enhancements of mid-energy and high-energy electron fluxes (purple arrows in Figures 2h and 2i). These electrons were mainly along 0° pitch angle, indicating that the magnetic topology in the leading part of the MH was changed from typical magnetosheath field lines (with neither end connected to the magnetosphere) to open field lines with one end connected to the southern magnetosphere. This is strong evidence that MFR and MH were interacting, causing magnetic reconnection at their interface.

4. Reconnection Signatures in the Current Sheet Formed Between MFR and MH

To identify signatures of magnetic reconnection in the current sheet, the data are transformed into a current sheet boundary normal (LMN) coordinate system. Here \mathbf{N} is determined by the maximum gradient direction of the magnetic field using the minimum directional derivative (MDD) method (Shi et al., 2005, 2019); $\mathbf{M} = \mathbf{N} \times \mathbf{L}'$, where \mathbf{L}' is the maximum variance direction from the MVA method, and $\mathbf{L} = \mathbf{M} \times \mathbf{N}$. The magnetic field data during the interval 03:25:16.0–03:25:16.3 UT is used for MDD and MVA methods.

Figure 3 shows MMS4 observations of the current sheet between MFR and MH in the LMN coordinate system. Here, $\mathbf{L} = (-0.815, -0.054, 0.576)_{\text{GSE}}$, $\mathbf{M} = (-0.124, -0.956, -0.266)_{\text{GSE}}$, and $\mathbf{N} = (0.565, -0.288, 0.773)_{\text{GSE}}$. The magnetic field B_L gradually reversed from about -40 nT (trailing part of the MFR) to about 15 nT (leading part of the MH) in Figure 3a. The speed of this current sheet is estimated to be 102 km/s along the normal direction, suggesting a width of about 214 km (between the first and third vertical dashed lines), $\sim 4.2 d_i$. The guide field B_M just outside the current sheet was about -35 nT, comparable to B_L . The density ratio across the current sheet was approximately 2.4 (10.7 cm^{-3} on the low-density side whereas 26.2 cm^{-3} on the high-density side). The high asymmetries in the magnetic field and plasma between the two sides indicate an asymmetric current sheet. At the leading edge of this current sheet, the ion flow V_{iL} increased from an ambient value of -20 to about 80 km/s at $\sim 03:25:14.5$ UT (Figure 3c). This positive V_{iL} enhancement was observed simultaneously with a negative B_L intensification. The anticorrelated variations in three components of the magnetic field and ion velocity (Figure S2 in Supporting Information S1) suggest this V_{iL} enhancement was consistent with the Alfvénic fluctuation propagating parallel to the background magnetic field. Considering the whole current sheet between the first and third vertical dashed lines, B_L and V_{iL} shows an anticorrelated change in $B_L < 0$ side and correlated change in $B_L > 0$ side. Just at the B_L reversal, MMS observed a shallow dip of V_{iL} , with $\Delta V_{iL} \approx -20$ km/s, relative to a background flow. The change in $B_L - V_{iL}$ correlation and negative enhancement of V_{iL} within the B_L reversal

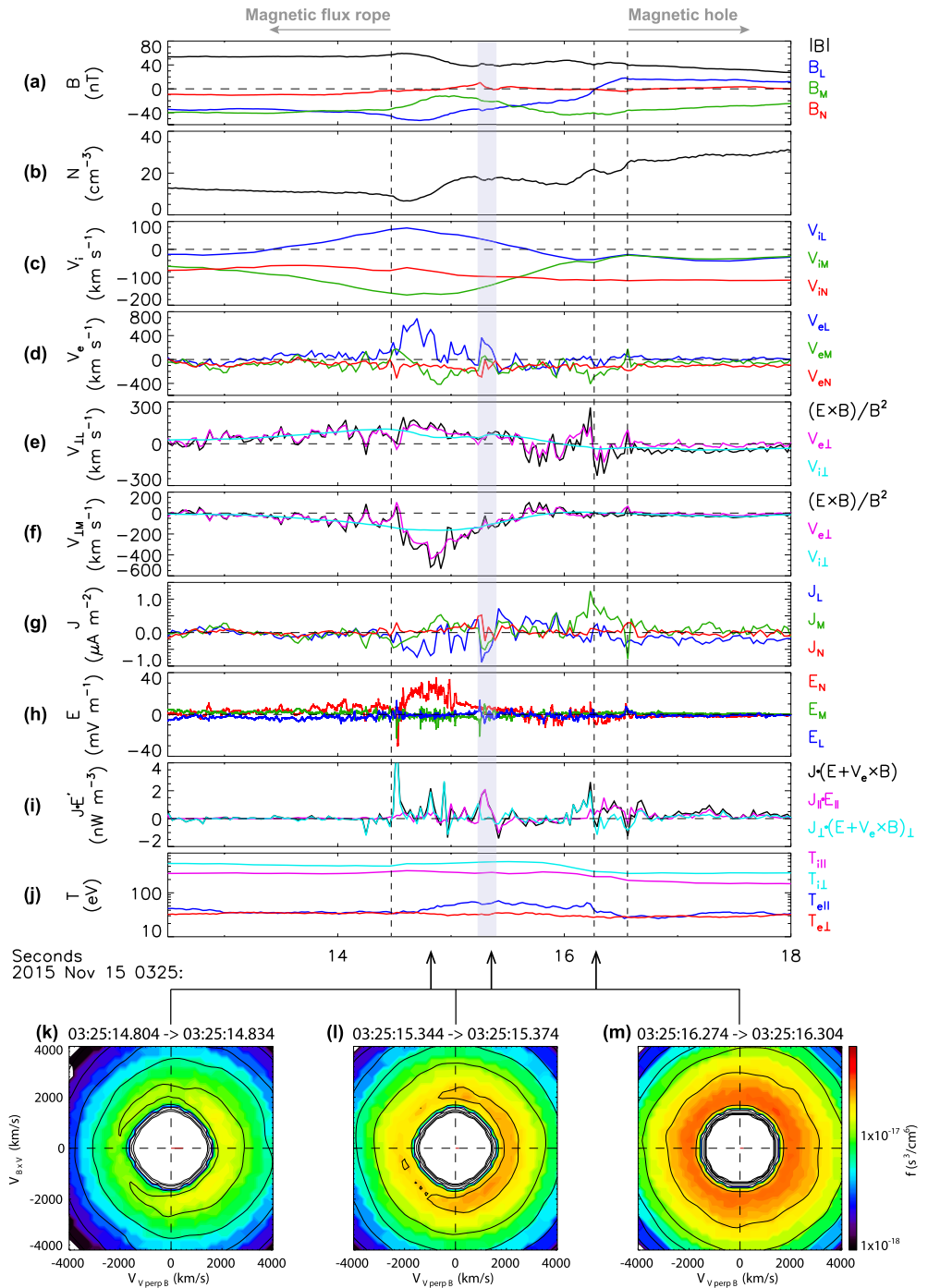


Figure 3. MMS4 observation of the reconnecting current sheet in the LMN coordinate system. Here $\mathbf{L} = (-0.815, -0.054, 0.576)_{GSE}$, $\mathbf{M} = (-0.124, -0.956, -0.266)_{GSE}$, and $\mathbf{N} = (0.565, -0.288, 0.773)_{GSE}$. (a) Magnetic field and its magnitude, (b) electron number density, (c) ion bulk velocity, (d) electron bulk velocity, (e)–(f) L and M components of $\mathbf{E} \times \mathbf{B}$ drift velocity, electron and ion perpendicular velocities, (g) current density, (h) electric field in the frame of the current sheet, (i) $\mathbf{J} \cdot \mathbf{E}' = \mathbf{J} \cdot (\mathbf{E} + \mathbf{V}_e \times \mathbf{B})$, (j) ion and electron temperatures in the parallel and perpendicular directions, and (k)–(m) electron velocity distributions in the plane perpendicular to the magnetic field.

region suggest MMS crossed the negative ion exhaust of the reconnecting current sheet, as shown in Figure 4b. This negative outflow was about $0.2 V_A$, where $V_A = 114$ km/s is the hybrid Alfvén speed derived in asymmetric reconnection $V_A^2 = B_{L1}B_{L2}(B_{L1} + B_{L2})/(\mu_0\rho_1B_{L2} + \mu_0\rho_2B_{L1})$ (Cassak & Shay, 2007), where subscripts 1 and 2 denote two sides of the current sheet.

During the crossing of this current sheet, B_M increased from about -35 nT to about -15 nT, and then decreased to about -45 nT before finally returning to the background field of -35 nT. This B_M variation is consistent with the asymmetric and bipolar Hall magnetic field on negative exhaust side of the reconnection with a high guide field (Eastwood et al., 2010). The positive Hall magnetic field was restricted within the negative B_L side and associated with the reversal of electron flow V_{eL} from positive to negative (Figure 3d). This positive V_{eL} at the leading edge of the positive Hall magnetic field region was up to 700 km/s ($\sim 6.1 V_A$) and could be the electron inflow at the separatrix region. In this inflow, the perpendicular electron velocity $V_{e\perp L}$ in Figure 3e was almost equal to $\mathbf{E} \times \mathbf{B}$ drift velocity (mainly from $E_N B_M$), but its value (~ 150 km/s) was smaller than the total inflow velocity. Thus the electron inflow was a combination of $\mathbf{E} \times \mathbf{B}$ drift velocity and field-aligned flow. Furthermore, the negative V_{eL} was measured at the trailing edge of the positive Hall magnetic field and corresponded to the outflowing electrons. These positive and negative electron flows shown by red arrows in Figure 4b constitute the Hall electron current system on the negative exhaust side. The change of J_L in Figure 3g also supports this current system. Figure 3h plots the electric field in the frame of the current sheet $\mathbf{E} = \mathbf{E}_{MMS} + \mathbf{V}_{CS} \times \mathbf{B}$, where \mathbf{E}_{MMS} is the electric field measured by MMS and \mathbf{V}_{CS} is the velocity of the current sheet frame relative to the MMS. The normal electric field E_N was mainly positive (up to 30 mV/m), that is, pointing toward the center of the current sheet, and was concentrated between 03:25:14.6 and 03:25:15.5 UT. This E_N was consistent with the unipolar Hall electric field in asymmetric reconnection. Conspicuously, a large negative dip of E_N was observed just prior to the Hall electric field. These magnetic and electric field observations provide evidence that MMS was crossing the ion diffusion region. This is also confirmed by the deviation between ion velocity and $\mathbf{E} \times \mathbf{B}$ drift velocity (Figures 3e and 3f), indicating that the ions were decoupled from the magnetic field.

Figure 3i shows the energy dissipation in the electron frame $\mathbf{J} \cdot \mathbf{E}' = \mathbf{J} \cdot (\mathbf{E} + \mathbf{V}_e \times \mathbf{B})$ (Zenitani et al., 2011). In the region with strong E_N (03:25:14.5–03:25:15.0 UT), $\mathbf{J} \cdot \mathbf{E}'$ was large (Eriksson et al., 2016; Wilder et al., 2018) and dominated by the perpendicular term, whereas around the midplane where $B_L = 0$, $\mathbf{J} \cdot \mathbf{E}'$ had comparable contributions from the perpendicular and parallel terms. Note that an isolated $J_{\parallel} E_{\parallel}$ peak was observed inside an electron current layer (shaded region) at $\sim 03:25:15.3$ UT. Positive $\mathbf{J} \cdot \mathbf{E}'$ indicates that the magnetic energy was dissipated and converted into plasma energy. The ion and electron temperatures were both increased inside this current sheet (Figure 3j), where ions were mainly heated in the perpendicular direction whereas electrons were heated in the parallel direction.

Figures 3k–3m present 2-D cuts of electron velocity distributions in the plane perpendicular to the magnetic field. The crescent-shaped electron distribution was distinct (Figure 3k) in the large E_N region which should be close to the separatrix. This crescent persisted into the exhaust region (Figure 3l) but was not visible after about 03:25:15.5 UT. This variation of the velocity distribution along the spacecraft trajectory (mainly in the \mathbf{N} direction) reveals the association between the crescent-shaped distribution and E_N (Bessho et al., 2016; Burch, Torbert, et al., 2016; X. M. Li et al., 2019). Near the midplane where E_N was small, the electron distribution became gyrotropic (Figure 3m).

As mentioned above, an unusual electron current layer (shaded region) with positive $J_{\parallel} E_{\parallel}$ peak was detected near the reversal point of bipolar V_{eL} at $\sim 03:25:15.3$ UT. The presence of E_{\parallel} (not shown) implies that the electron frozen-in condition $\mathbf{E} + \mathbf{V}_e \times \mathbf{B} = 0$ was violated therein. The width of this current layer was about 15.3 km, $\sim 0.3 d_p$, much narrower than the exhaust region. The J_M within this current layer was negative, opposite to regular J_M , for example, around the midplane where positive J_M was up to $1.2 \mu\text{A}/\text{m}^2$, which supports the reversal of reconnecting magnetic fields. The negative J_M was caused by the localized decrease of V_{eM} strength. Here V_{eM} was almost equal to $\mathbf{E} \times \mathbf{B}$ drift velocity ($V_{eM} \approx E_N B_L$) in Figure 3f, and thus a local dip of E_N to ~ 1.3 mV/m observed at $\sim 03:25:15.30$ UT caused the reduced strength of V_{eM} . Furthermore, high-speed electron flow V_{eL} was detected within this current layer. Its speed was as large as ~ 350 km/s, $\sim 3.1 V_A$. Since E_N was about 5 mV/m at $\sim 03:25:15.27$ UT where the largest V_{eL} was observed, the L component of $\mathbf{E} \times \mathbf{B}$ drift velocity contributed only approximately 20% to V_{eL} . Therefore, this positive V_{eL} was mainly field-aligned. The electric fields E_L and E_M also showed localized variations in this current layer. The E_M (E_L) had a negative dip (positive peak) bounded by a positive peak (negative dip) within the shaded region. The positive $\mathbf{J} \cdot \mathbf{E}'$ inside this current layer was mainly

caused by the high-speed electron jet (J_L) and parallel electric field in the **L** direction (E'_L). In contrast, $J_M E'_M$ was negative inside this current layer. Combining these observations, this $J_M < 0$ current layer embedded in the large-scale current sheet involves a few typical properties of the electron diffusion region (EDR) such as non-frozen-in electrons, positive $\mathbf{J} \cdot \mathbf{E}'$, and crescent-shaped electron distribution. However, the opposite out-of-plane current implies that the current layer was not the inner region of the EDR. Considering that this current layer was detected inside a much broader reconnection exhaust, this electron dissipation channel likely extends to the X-line, similar to an elongated EDR extending into the exhaust region (Le et al., 2013; Shay et al., 2007), as shown by the purple bar in Figure 4b.

5. Discussion and Conclusions

In this study, we report simultaneous MMS observations of MFR and MHs in the magnetosheath. The observed MFR could be generated by magnetopause reconnection since its magnetic field lines were connected to the magnetosphere. Previous studies have shown that the occurrence of MFRs at dayside magnetopause mainly corresponds to southward interplanetary magnetic field (Berchem & Russell, 1984; Kuo et al., 1995). In our event, the MFR existed in primarily northward magnetosheath magnetic field. However, a brief southward B_z in the magnetosheath was observed prior to the MFR. This southward B_z may cause the formation of the MFR. Previous statistical studies revealed that magnetosheath MFRs and magnetospheric MFRs can be the same physical phenomenon at the dayside magnetopause, with magnetosheath MFRs having more occurrence frequency (Kuo et al., 1995). This was possibly caused by the motion of MFRs sunward into the magnetosheath due to stronger curvature forces in the magnetosphere than in the magnetosheath. An intriguing question is whether these MFRs will dissipate in the turbulent magnetosheath environment. If this is the case, such dissipation could affect the transfer of mass, momentum, and energy from the solar wind into the magnetosphere.

A typical example of the dissipation of MFR occurs in the magnetotail. Slavin et al. (2003) first proposed that earthward-moving MFRs in the plasma sheet could dissipate quickly due to the reconnection with the northward geomagnetic field. This reconnection causes the southward B_z in the leading edge of MFR to dissipate and may explain some signatures of dipolarization fronts (Fu et al., 2012; Runov et al., 2011). This process has been studied by global hybrid simulations (S. Lu et al., 2015) and demonstrated by spacecraft observations (Man et al., 2018; Poh et al., 2019). However, the dissipation of MFRs at the dayside magnetopause is rarely observed.

In this paper, we provide a new scenario for the evolution of MFRs generated near the subsolar magnetopause. Based on the statistical study by Y. L. Wang et al. (2005), these MFRs could have a motion from inside the magnetopause toward the magnetosheath when propagating to the high-latitude magnetopause. The magnetosheath part of the MFRs can interact with the surrounding MHs through reconnection, which causes the magnetic fields of the MFRs to dissipate or erode. Given that the magnetosheath is permeated with large numbers of MHs (Balikhin et al., 2009; S. Y. Huang et al., 2017; Liu et al., 2019; Yao et al., 2017) where the plasma properties are in general favorable for excitation of mirror instability, MFRs can dissipate through reconnection with multiple MHs. On the other hand, the MHs that were abundant in the magnetosheath can merge into the magnetopause through this reconnection. Based on MMS observations, we provide direct evidence of reconnection between MFR and MH, which has a pivotal role in this scenario. Recent numerical studies have found the coexistence of MFRs at the magnetopause and mirror mode MHs in the magnetosheath (Z. F. Guo et al., 2020; Hoilijoki et al., 2017), which supports this scenario. In these simulations, however, the interaction between MFRs and MHs is not found. The ultimate fate of these MFRs is to disintegrate in the cusp (Omidi & Sibeck, 2007). Our results provide another fate in which MFRs can dissipate in the magnetosheath through reconnection with MHs. This process is somewhat similar to the magnetic cloud erosion by reconnection with the ambient interplanetary magnetic field (Dasso et al., 2006; Ruffenach et al., 2012; R. S. Wang et al., 2023).

It should be noted that the southward B_z of the MFR would have antiparallel magnetic fields with magnetosheath northward B_z regardless of the presence of MHs. Therefore, the reconnection between MFR and magnetosheath magnetic field is expected and could also dissipate the MFR. The necessary condition for this reconnection triggering is the compression to form a thin current sheet (Phan, Paschmann, et al., 2007). In our event, the MFR mainly moves along the $-\mathbf{Z}_{GSE}$ direction, therefore the convective compression due to the flows in the magnetosheath (Z. Guo et al., 2021; Pang et al., 2010) could be weak, which may restrict the thinning of the current sheet to trigger reconnection if only magnetosheath magnetic field is considered. For the current sheet between MFR and MH in our event, the local magnetic field enhancement was observed on both sides of the current sheet,

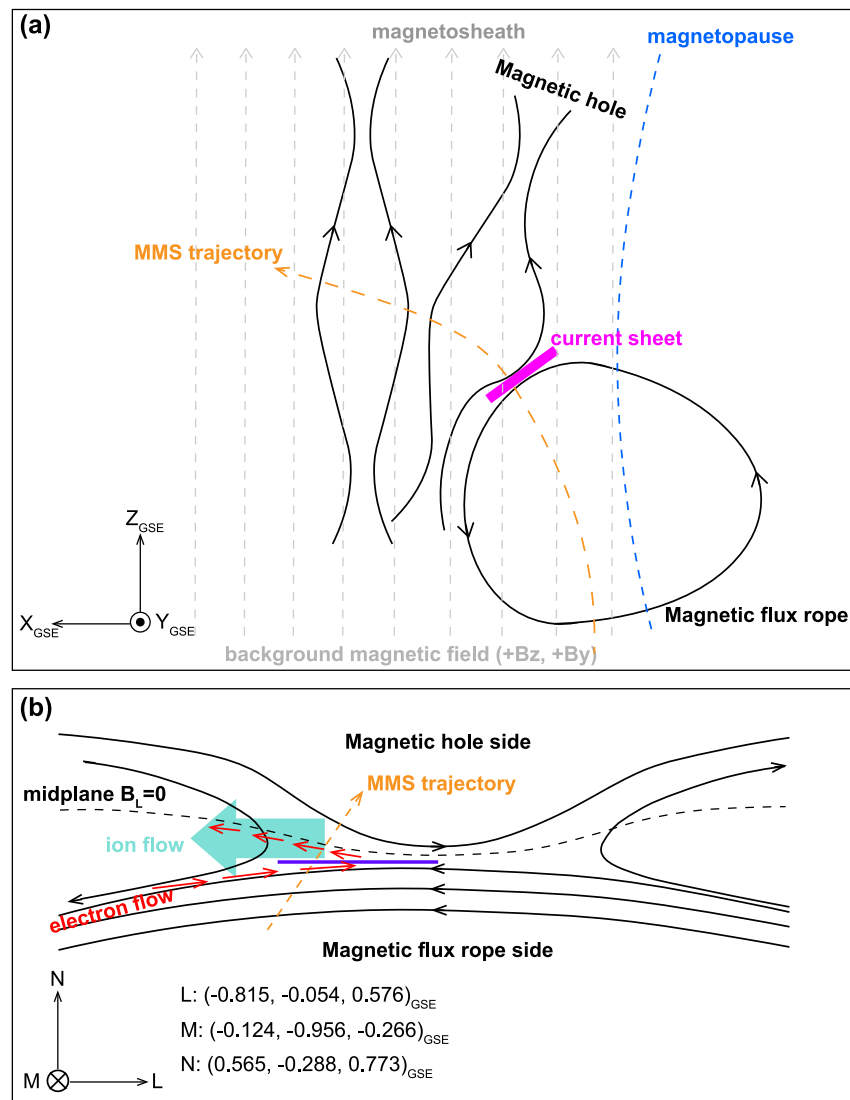


Figure 4. 2-D sketches summarizing the main structures and processes observed by the MMS. (a) A sketch of the spacecraft trajectory through magnetic flux rope, magnetic hole, and the current sheet between them, and (b) a sketch of the spacecraft trajectory through the reconnecting current sheet.

which is favorable for the formation of a thin current sheet. Therefore the MH may be important in triggering the reconnection at the boundary of the MFR. One potential reason is the magnetic field configuration of the MH as shown in Figure 4a. The evidence that supports this conjecture is the reconnecting magnetic field B_L in our event is along the $(-0.815, -0.054, 0.576)_{GSE}$ direction, dominated by the X_{GSE} direction, not the Z_{GSE} direction. Another possible reason is the propagating property of the MH (Yao et al., 2020). The MH in our event was 1-D, with leading part moving earthward and trailing part moving sunward (Figure S3 in Supporting Information S1), implying an expanding nature, which is favorable for the compression of the current sheet between MH and MFR.

At the interface of MFR and MH, MMS crossed a current sheet in which typical reconnection signatures were observed. This reconnection event is a typical asymmetric reconnection with a high guide field (Eriksson et al., 2016; Wilder et al., 2018). A noteworthy point is that an elongated EDR embedded in the reconnection exhaust was detected. This elongated EDR has some different features from previous studies (Hwang et al., 2017; Phan, Drake, et al., 2007; S. M. Wang et al., 2021; Zhong et al., 2020), for example, positive $\mathbf{J} \cdot \mathbf{E}'$ (a combination of positive $J_L E'_L$ and negative $J_M E'_M$) and anomalous out-of-plane current. These results are important complements to the reconnection study in different regimes.

In conclusion, the paper presents an in situ observation of reconnection between MFR and MH in the magnetosheath. This reconnection can cause the MFR to dissipate, and also the MH to merge into the magnetopause. Such a process may not be rare since they are both common structures in the magnetosheath. Future studies, especially numerical simulations, are needed to reveal their roles in the coupling between the solar wind and the magnetosphere.

Data Availability Statement

The MMS data used in this work are available at the MMS data center (<https://lasp.colorado.edu/mms/sdc/public/about/browse-wrapper/>). The OMNI data are available at NASA's SPDF OMNIWeb Service (<https://omniweb.gsfc.nasa.gov/>).

Acknowledgments

We thank the entire MMS team for providing such excellent and well calibrated data that permits this study. This work is supported by the National Science Foundation of China (NSFC) Grants (41922030, 42174181, and 42174187), the Project funded by China Postdoctoral Science Foundation (2023M743356), the Postdoctoral Fellowship Program of CPSF, the Fundamental Research Funds for the Central Universities, and the Xiaomi Young Talents Program.

References

- Akhavan-Tafti, M., Slavin, J. A., Eastwood, J. P., Cassak, P. A., & Gershman, D. J. (2019). MMS multi-point analysis of FTE evolution: Physical characteristics and dynamics. *Journal of Geophysical Research: Space Physics*, *124*(7), 5376–5395. <https://doi.org/10.1029/2018ja026311>
- Akhavan-Tafti, M., Slavin, J. A., Le, G., Eastwood, J. P., Strangeway, R. J., Russell, C. T., et al. (2018). MMS examination of FTEs at the Earth's subsolar magnetopause. *Journal of Geophysical Research: Space Physics*, *123*(2), 1224–1241. <https://doi.org/10.1002/2017ja024681>
- Balikhin, M. A., Sagdeev, R. Z., Walker, S. N., Pokhotelov, O. A., Sibeck, D. G., Beloff, N., & Dudnikova, G. (2009). THEMIS observations of mirror structures: Magnetic holes and instability threshold. *Geophysical Research Letters*, *36*(3). <https://doi.org/10.1029/2008gl036923>
- Berchem, J., & Russell, C. T. (1984). Flux transfer events on the magnetopause: Spatial distribution and controlling factors. *Journal of Geophysical Research*, *89*(A8), 6689–6703. <https://doi.org/10.1029/ja089ia08p06689>
- Bessho, N., Chen, L. J., & Hesse, M. (2016). Electron distribution functions in the diffusion region of asymmetric magnetic reconnection. *Geophysical Research Letters*, *43*(5), 1828–1836. <https://doi.org/10.1002/2016gl067886>
- Burch, J. L., Moore, T. E., Torbert, R. B., & Giles, B. L. (2016). Magnetospheric Multiscale overview and science objectives. *Space Science Reviews*, *199*(1–4), 5–21. <https://doi.org/10.1007/s11214-015-0164-9>
- Burch, J. L., Torbert, R. B., Phan, T. D., Chen, L. J., Moore, T. E., Ergun, R. E., et al. (2016). Electron-scale measurements of magnetic reconnection in space. *Science*, *352*(6290). <https://doi.org/10.1126/science.aaf2939>
- Cassak, P. A., & Shay, M. A. (2007). Scaling of asymmetric magnetic reconnection: General theory and collisional simulations. *Physics of Plasmas*, *14*(10). <https://doi.org/10.1063/1.2795630>
- Chen, Z. Z., Fu, H. S., Wang, Z., Guo, Z. Z., Xu, Y., & Liu, C. M. (2021). First observation of magnetic flux rope inside electron diffusion region. *Geophysical Research Letters*, *48*(7). <https://doi.org/10.1029/2020gl089722>
- Dasso, S., Mandrini, C. H., Démoulin, P., & Luoni, M. L. (2006). A new model-independent method to compute magnetic helicity in magnetic clouds. *Astronomy and Astrophysics*, *455*(1), 349–359. <https://doi.org/10.1051/0004-6361:20064806>
- Daughton, W., Roytershteyn, V., Karimabadi, H., Yin, L., Albright, B. J., Bergen, B., & Bowers, K. J. (2011). Role of electron physics in the development of turbulent magnetic reconnection in collisionless plasmas. *Nature Physics*, *7*(7), 539–542. <https://doi.org/10.1038/nphys1965>
- Daughton, W., Scudder, J., & Karimabadi, H. (2006). Fully kinetic simulations of undriven magnetic reconnection with open boundary conditions. *Physics of Plasmas*, *13*(7). <https://doi.org/10.1063/1.2218817>
- Dong, X. C., Dunlop, M. W., Trattner, K. J., Phan, T. D., Fu, H., Cao, J., et al. (2017). Structure and evolution of flux transfer events near dayside magnetic reconnection dissipation region: MMS observations. *Geophysical Research Letters*, *44*(12), 5951–5959. <https://doi.org/10.1002/2017gl073411>
- Drake, J. F., Swisdak, M., Schoeffler, K. M., Rogers, B. N., & Kobayashi, S. (2006). Formation of secondary islands during magnetic reconnection. *Geophysical Research Letters*, *33*(13). <https://doi.org/10.1029/2006gl029597>
- Eastwood, J. P., Phan, T. D., Cassak, P. A., Gershman, D. J., Haggerty, C., Malakit, K., et al. (2016). Ion-scale secondary flux ropes generated by magnetopause reconnection as resolved by MMS. *Geophysical Research Letters*, *43*(10), 4716–4724. <https://doi.org/10.1002/2016gl068747>
- Eastwood, J. P., Phan, T. D., Fear, R. C., Sibeck, D. G., Angelopoulos, V., Oieroset, M., & Shay, M. A. (2012). Survival of flux transfer event (FTE) flux ropes far along the tail magnetopause. *Journal of Geophysical Research*, *117*(A8). <https://doi.org/10.1029/2012ja017722>
- Eastwood, J. P., Phan, T. D., Mozer, F. S., Shay, M. A., Fujimoto, M., Retinò, A., et al. (2007). Multi-point observations of the Hall electromagnetic field and secondary island formation during magnetic reconnection. *Journal of Geophysical Research*, *112*(A6). <https://doi.org/10.1029/2006ja012158>
- Eastwood, J. P., Shay, M. A., Phan, T. D., & Oieroset, M. (2010). Asymmetry of the ion diffusion region hall electric and magnetic fields during guide field reconnection: Observations and comparison with simulations. *Physical Review Letters*, *104*(20), 205001. <https://doi.org/10.1103/physrevlett.104.205001>
- Ergun, R. E., Tucker, S., Westfall, J., Goodrich, K. A., Malaspina, D. M., Summers, D., et al. (2016). The axial double probe and fields signal processing for the MMS mission. *Space Science Reviews*, *199*(1–4), 167–188. https://doi.org/10.1007/978-94-024-0861-4_7
- Eriksson, S., Wilder, F. D., Ergun, R. E., Schwartz, S. J., Cassak, P. A., Burch, J. L., et al. (2016). Magnetospheric multiscale observations of the electron diffusion region of large guide field magnetic reconnection. *Physical Review Letters*, *117*(1), 015001. <https://doi.org/10.1103/physrevlett.117.015001>
- Fear, R. C., Milan, S. E., Fazakerley, A. N., Lucek, E. A., Cowley, S. W. H., & Dandouras, I. (2008). The azimuthal extent of three flux transfer events. *Annales Geophysicae*, *26*(8), 2353–2369. <https://doi.org/10.5194/angeo-26-2353-2008>
- Fear, R. C., Milan, S. E., Fazakerley, A. N., Owen, C. J., Asikainen, T., Taylor, M. G. T., et al. (2007). Motion of flux transfer events: A test of the cooling model. *Annales Geophysicae*, *25*(7), 1669–1690. <https://doi.org/10.5194/angeo-25-1669-2007>
- Fear, R. C., Milan, S. E., & Oksavik, K. (2012). Determining the axial direction of high-shear flux transfer events: Implications for models of FTE structure. *Journal of Geophysical Research*, *117*(A9), A09220. <https://doi.org/10.1029/2012ja017831>
- Fu, H. S., Khotyaintsev, Y. V., Vaivads, A., André, M., & Huang, S. Y. (2012). Occurrence rate of earthward-propagating dipolarization fronts. *Geophysical Research Letters*, *39*(10). <https://doi.org/10.1029/2012gl051784>
- Fu, H. S., Vaivads, A., Khotyaintsev, Y. V., Andre, M., Cao, J. B., Olshevsky, V., et al. (2017). Intermittent energy dissipation by turbulent reconnection. *Geophysical Research Letters*, *44*(1), 37–43. <https://doi.org/10.1002/2016gl071787>

- Génot, V., Schwartz, S. J., Mazelle, C., Balikhin, M., Dunlop, M., & Bauer, T. M. (2001). Kinetic study of the mirror mode. *Journal of Geophysical Research*, 106(A10), 21611–21622. <https://doi.org/10.1029/2000ja000457>
- Guo, J., Lu, S., Lu, Q. M., Lin, Y., Wang, X. Y., Huang, K., et al. (2021). Structure and coalescence of magnetopause flux ropes and their dependence on IMF clock angle: Three-dimensional global hybrid simulations. *Journal of Geophysical Research: Space Physics*, 126(2). <https://doi.org/10.1029/2020ja028670>
- Guo, Z., Lin, Y., & Wang, X. (2021). Global hybrid simulations of interaction between interplanetary rotational discontinuity and bow shock/magnetosphere: Can ion-scale magnetic reconnection be driven by rotational discontinuity downstream of quasi-parallel shock? *Journal of Geophysical Research: Space Physics*, 126(4), e2020JA028853. <https://doi.org/10.1029/2020ja028853>
- Guo, Z. F., Lin, Y., Wang, X. Y., Vines, S. K., Lee, S. H., & Chen, Y. X. (2020). Magnetopause reconnection as influenced by the dipole tilt under southward IMF conditions: Hybrid simulation and MMS observation. *Journal of Geophysical Research: Space Physics*, 125(9). <https://doi.org/10.1029/2020ja027795>
- Hasegawa, A. (1969). Drift mirror instability in the magnetosphere. *Physics of Fluids*, 12, 2642–2650. <https://doi.org/10.1063/1.1692407>
- Hasegawa, H., Denton, R. E., Dokgo, K., Hwang, K. J., Nakamura, T. K. M., & Burch, J. L. (2023). Ion-scale magnetic flux rope generated from electron-scale magnetopause current sheet: Magnetospheric Multiscale observations. *Journal of Geophysical Research: Space Physics*, 128(3). <https://doi.org/10.1029/2022ja031092>
- Hasegawa, H., Kitamura, N., Saito, Y., Nagai, T., Shinohara, I., Yokota, S., et al. (2016). Decay of mesoscale flux transfer events during quasi-continuous spatially extended reconnection at the magnetopause. *Geophysical Research Letters*, 43(10), 4755–4762. <https://doi.org/10.1002/2016gl069225>
- Hasegawa, H., Wang, J., Dunlop, M. W., Pu, Z. Y., Zhang, Q., Lavraud, B., et al. (2010). Evidence for a flux transfer event generated by multiple X-line reconnection at the magnetopause. *Geophysical Research Letters*, 37(16). <https://doi.org/10.1029/2010gl044219>
- Hoilijoki, S., Ganse, U., Pfau-Kempf, Y., Cassak, P. A., Walsh, B. M., Hietala, H., et al. (2017). Reconnection rates and X line motion at the magnetopause: Global 2D-3V hybrid-vlasov simulation results. *Journal of Geophysical Research: Space Physics*, 122(3), 2877–2888. <https://doi.org/10.1002/2016ja023709>
- Horbury, T. S., Lucek, E. A., Balogh, A., Dandouras, I., & Rème, H. (2004). Motion and orientation of magnetic field dips and peaks in the terrestrial magnetosheath. *Journal of Geophysical Research*, 109(A9). <https://doi.org/10.1029/2003ja010237>
- Huang, C., Lu, Q., Yang, Z., Wu, M., Dong, Q., & Wang, S. (2011). The evolution of electron current sheet and formation of secondary islands in guide field reconnection. *Nonlinear Processes in Geophysics*, 18(5), 727–733. <https://doi.org/10.5194/npg-18-727-2011>
- Huang, C., Lu, Q. M., Wang, R. S., Guo, F., Wu, M. Y., Lu, S., & Wang, S. (2017). Development of turbulent magnetic reconnection in a magnetic island. *The Astrophysical Journal*, 835(2), 245. <https://doi.org/10.3847/1538-4357/835/2/245>
- Huang, S. Y., Du, J. W., Sahraoui, F., Yuan, Z. G., He, J. S., Zhao, J. S., et al. (2017). A statistical study of kinetic-size magnetic holes in turbulent magnetosheath: MMS observations. *Journal of Geophysical Research: Space Physics*, 122(8), 8577–8588. <https://doi.org/10.1002/2017ja024415>
- Huang, S. Y., Jiang, K., Yuan, Z. G., Zhou, M., Sahraoui, F., Fu, H. S., et al. (2019). Observations of flux ropes with strong energy dissipation in the magnetotail. *Geophysical Research Letters*, 46(2), 580–589. <https://doi.org/10.1029/2018gl081099>
- Hwang, K. J., Sibeck, D. G., Burch, J. L., Choi, E., Fear, R. C., Lavraud, B., et al. (2018). Small-scale flux transfer events formed in the reconnection exhaust region between two X lines. *Journal of Geophysical Research: Space Physics*, 123(10), 8473–8488. <https://doi.org/10.1029/2018ja025611>
- Hwang, K. J., Sibeck, D. G., Choi, E., Chen, L., Ergun, R. E., Khotyaintsev, Y., et al. (2017). Magnetospheric Multiscale mission observations of the outer electron diffusion region. *Geophysical Research Letters*, 44(5), 2049–2059. <https://doi.org/10.1002/2017gl072830>
- Hwang, K. J., Sibeck, D. G., Giles, B. L., Pollock, C. J., Gershman, D., Avakov, L., et al. (2016). The substructure of a flux transfer event observed by the MMS spacecraft. *Geophysical Research Letters*, 43(18), 9434–9443. <https://doi.org/10.1002/2016gl070934>
- Kuo, H., Russell, C. T., & Le, G. (1995). Statistical studies of flux transfer events. *Journal of Geophysical Research*, 100(A3), 3513–3519. <https://doi.org/10.1029/94ja02498>
- Laitinen, T. V., Khotyaintsev, Y. V., André, M., Vaivads, A., & Rème, H. (2010). Local influence of magnetosheath plasma beta fluctuations on magnetopause reconnection. *Annales Geophysicae*, 28(5), 1053–1063. <https://doi.org/10.5194/angeo-28-1053-2010>
- Le, A., Egedal, J., Ohia, O., Daughton, W., Karimabadi, H., & Lukin, V. S. (2013). Regimes of the electron diffusion region in magnetic reconnection. *Physical Review Letters*, 110(13), 135004. <https://doi.org/10.1103/physrevlett.110.135004>
- Lee, L. C., & Fu, Z. F. (1985). A theory of magnetic flux transfer at the Earth's magnetopause. *Geophysical Research Letters*, 12(2), 105–108. <https://doi.org/10.1029/gl012i002p00105>
- Li, J. H., Zhou, X. Z., Zong, Q. G., Yang, F., Fu, S. Y., Yao, S. T., et al. (2021). On the origin of donut-shaped electron distributions within magnetic cavities. *Geophysical Research Letters*, 48(2). <https://doi.org/10.1029/2020gl091613>
- Li, X. M., Wang, R. S., Lu, Q. M., Hwang, Y. O. O., Zong, Q. G., Russell, C. T., & Wang, S. (2019). Observation of nongyrotropic electron distribution across the electron diffusion region in the magnetotail reconnection. *Geophysical Research Letters*, 46(24), 14263–14273. <https://doi.org/10.1029/2019gl085014>
- Lindqvist, P. A., Olsson, G., Torbert, R. B., King, B., Granoff, M., Rau, D., et al. (2016). The spin-plane double probe electric field instrument for MMS. *Space Science Reviews*, 199(1–4), 137–165. https://doi.org/10.1007/978-94-024-0861-4_6
- Liu, H., Zong, Q. G., Zhang, H., Xiao, C. J., Shi, Q. Q., Yao, S. T., et al. (2019). MMS observations of electron scale magnetic cavity embedded in proton scale magnetic cavity. *Nature Communications*, 10(1), 1040. <https://doi.org/10.1038/s41467-019-08971-y>
- Lu, Q. M., Huang, K., Guan, Y. D., Lu, S., & Wang, R. S. (2023). Energy dissipation in magnetic islands formed during magnetic reconnection. *The Astrophysical Journal*, 954(2), 146. <https://doi.org/10.3847/1538-4357/acea86>
- Lu, S., Angelopoulos, V., Artemyev, A. V., Pritchett, P. L., Liu, J., Runov, A., et al. (2019). Turbulence and particle acceleration in collisionless magnetic reconnection: Effects of temperature inhomogeneity across pre-reconnection current sheet. *The Astrophysical Journal*, 878(2), 109. <https://doi.org/10.3847/1538-4357/ab1f6b>
- Lu, S., Lu, Q., Lin, Y., Wang, X., Ge, Y., Wang, R., et al. (2015). Dipolarization fronts as earthward propagating flux ropes: A three-dimensional global hybrid simulation. *Journal of Geophysical Research: Space Physics*, 120(8), 6286–6300. <https://doi.org/10.1002/2015ja021213>
- Lucek, E. A., Dunlop, M. W., Horbury, T. S., Balogh, A., Brown, P., Cargill, P., et al. (2001). Cluster magnetic field observations in the magnetosheath: Four-point measurements of mirror structures. *Annales Geophysicae*, 19(10/12), 1421–1428. <https://doi.org/10.5194/angeo-19-1421-2001>
- Man, H. Y., Zhou, M., Deng, X. H., Fu, H. S., Zhong, Z. H., Chen, Z. Z., et al. (2018). In situ observation of magnetic reconnection between an earthward propagating flux rope and the geomagnetic field. *Geophysical Research Letters*, 45(17), 8729–8737. <https://doi.org/10.1029/2018gl079778>

- Øieroset, M., Phan, T. D., Eastwood, J. P., Fujimoto, M., Daughton, W., Shay, M. A., et al. (2011). Direct evidence for a three-dimensional magnetic flux rope flanked by two active magnetic reconnection X lines at Earth's magnetopause. *Physical Review Letters*, 107(16), 165007. <https://doi.org/10.1103/physrevlett.107.165007>
- Øieroset, M., Phan, T. D., Haggerty, C., Shay, M. A., Eastwood, J. P., Gershman, D. J., et al. (2016). MMS observations of large guide field symmetric reconnection between colliding reconnection jets at the center of a magnetic flux rope at the magnetopause. *Geophysical Research Letters*, 43(11), 5536–5544. <https://doi.org/10.1002/2016gl069166>
- Omidi, N., & Sibeck, D. G. (2007). Flux transfer events in the cusp. *Geophysical Research Letters*, 34(4). <https://doi.org/10.1029/2006gl028698>
- Owen, C. J., Fazakerley, A. N., Carter, P. J., Coates, A. J., Krauklis, I. C., Szita, S., et al. (2001). Cluster PEACE observations of electrons during magnetospheric flux transfer events. *Annales Geophysicae*, 19(10–12), 1509–1522. <https://doi.org/10.5194/angeo-19-1509-2001>
- Pang, Y., Lin, Y., Deng, X. H., Wang, X. Y., & Tan, B. (2010). Three-dimensional hybrid simulation of magnetosheath reconnection under northward and southward interplanetary magnetic field. *Journal of Geophysical Research*, 115(A3), A03203. <https://doi.org/10.1029/2009ja014415>
- Phan, T. D., Drake, J. F., Shay, M. A., Mozer, F. S., & Eastwood, J. P. (2007). Evidence for an elongated (>60 ion skin depths) electron diffusion region during fast magnetic reconnection. *Physical Review Letters*, 99(25), 255002. <https://doi.org/10.1103/physrevlett.99.255002>
- Phan, T. D., Paschmann, G., Twitty, C., Mozer, F. S., Gosling, J. T., Eastwood, J. P., et al. (2007). Evidence for magnetic reconnection initiated in the magnetosheath. *Geophysical Research Letters*, 34(14), L14104. <https://doi.org/10.1029/2007gl030343>
- Poh, G., Slavin, J. A., Lu, S., Le, G., Ozturk, D. S., Sun, W., et al. (2019). Dissipation of earthward propagating flux rope through re-connection with geomagnetic field: An MMS case study. *Journal of Geophysical Research: Space Physics*, 124(9), 7477–7493. <https://doi.org/10.1029/2018ja026451>
- Pollock, C., Moore, T., Jacques, A., Burch, J., Gliese, U., Saito, Y., et al. (2016). Fast plasma investigation for magnetospheric multiscale. *Space Science Reviews*, 199(1–4), 331–406. <https://doi.org/10.1007/s11214-016-0245-4>
- Pu, Z. Y., Raeder, J., Zhong, J., Bogdanova, Y. V., Dunlop, M., Xiao, C. J., et al. (2013). Magnetic topologies of an in vivo FTE observed by Double Star/TC-1 at Earth's magnetopause. *Geophysical Research Letters*, 40(14), 3502–3506. <https://doi.org/10.1002/grl.50714>
- Raeder, J. (2006). Flux transfer events: I. Generation mechanism for strong southward IMF. *Annales Geophysicae*, 24(1), 381–392. <https://doi.org/10.5194/angeo-24-381-2006>
- Ruffenach, A., Lavraud, B., Owens, M. J., Sauvaud, J., Savani, N. P., Rouillard, A. P., et al. (2012). Multispacecraft observation of magnetic cloud erosion by magnetic reconnection during propagation. *Journal of Geophysical Research*, 117(A9). <https://doi.org/10.1029/2012ja017624>
- Runov, A., Angelopoulos, V., Zhou, X. Z., Zhang, X. J., Li, S., Plaschke, F., & Bonnell, J. (2011). A THEMIS multicase study of dipolarization fronts in the magnetotail plasma sheet. *Journal of Geophysical Research*, 116(A5). <https://doi.org/10.1029/2010ja016316>
- Russell, C. T., Anderson, B. J., Baumjohann, W., Bromund, K. R., Dearborn, D., Fischer, D., et al. (2016). The magnetospheric multiscale magnetometers. *Space Science Reviews*, 199(1–4), 189–256. https://doi.org/10.1007/978-94-024-0861-4_8
- Russell, C. T., & Elphic, R. C. (1978). Initial ISEE magnetometer results: Magnetopause observations. *Space Science Reviews*, 22(6), 681–715. <https://doi.org/10.1007/bf00212619>
- Schwartz, S. J. (1998). Shock and discontinuity normals, mach numbers and related parameters. In G. Paschmann & P. W. Daly (Eds.), *Analysis methods for multi-spacecraft data* (pp. 249–270). International Space Science Institute.
- Shay, A., Drake, J. F., & Swisdak, M. (2007). Two-scale structure of the electron dissipation region during collisionless magnetic reconnection. *Physical Review Letters*, 99(15), 155002. <https://doi.org/10.1103/physrevlett.99.155002>
- Shi, Q. Q., Shen, C., Pu, Z. Y., Dunlop, M. W., Zong, Q. G., Zhang, H., et al. (2005). Dimensional analysis of observed structures using multipoint magnetic field measurements: Application to cluster. *Geophysical Research Letters*, 32(12). <https://doi.org/10.1029/2005gl022454>
- Shi, Q. Q., Tian, A. M., Bai, S. C., Hasegawa, H., Degeling, A. W., Pu, Z. Y., et al. (2019). Dimensionality, coordinate system and reference frame for analysis of in-situ space plasma and field data. *Space Science Reviews*, 215(4), 35. <https://doi.org/10.1007/s11214-019-0601-2>
- Slavin, J. A., Lepping, R. P., Gjerloev, J., Fairfield, D. H., Hesse, M., Owen, C. J., et al. (2003). Geotail observations of magnetic flux ropes in the plasma sheet. *Journal of Geophysical Research*, 108(A1). <https://doi.org/10.1029/2002ja009557>
- Sonnerup, B., & Scheible, M. (1998). Analysis methods for multi-spacecraft data. *ISSI Scientific Report*.
- Soucek, J., Lucek, E., & Dandouras, I. (2008). Properties of magnetosheath mirror modes observed by Cluster and their response to changes in plasma parameters. *Journal of Geophysical Research*, 113(A4). <https://doi.org/10.1029/2007ja012649>
- Teh, W. L., Denton, R. E., Sonnerup, B. U. O., & Pollock, C. (2017). MMS observations of oblique small-scale magnetopause flux ropes near the ion diffusion region during weak guide-field reconnection. *Geophysical Research Letters*, 44(13), 6517–6524. <https://doi.org/10.1002/2017gl074291>
- Tsurutani, B. T., Smith, E. J., Anderson, R. R., Ogilvie, K. W., Scudder, J. D., Baker, D. N., & Bame, S. J. (1982). Lion roars and nonoscillatory drift mirror waves in the magnetosheath. *Journal of Geophysical Research*, 87(A8), 6060–6072. <https://doi.org/10.1029/ja087ia08p06060>
- Wang, R. S., Cheng, Z., Slavin, J. A., Lu, Q., Raines, J., Lu, S., et al. (2024). Direct detection of ongoing magnetic reconnection at Mercury's high-latitude magnetopause. *Geophysical Research Letters*, 51(5), e2023GL106282. <https://doi.org/10.1029/2023gl106282>
- Wang, R. S., Lu, Q., Nakamura, R., Baumjohann, W., Russell, C. T., Burch, J. L., et al. (2017). Interaction of magnetic flux ropes via magnetic reconnection observed at the magnetopause. *Journal of Geophysical Research: Space Physics*, 122(10), 10436–10447. <https://doi.org/10.1002/2017ja024482>
- Wang, R. S., Lu, Q. M., Du, A. M., & Wang, S. (2010). In situ observations of a secondary magnetic island in an ion diffusion region and associated energetic electrons. *Physical Review Letters*, 104(17), 175003. <https://doi.org/10.1103/physrevlett.104.175003>
- Wang, R. S., Lu, Q. M., Li, X., Huang, C., & Wang, S. (2010). Observations of energetic electrons up to 200 keV associated with a secondary island near the center of an ion diffusion region: A cluster case study. *Journal of Geophysical Research*, 115(A11). <https://doi.org/10.1029/2010ja015473>
- Wang, R. S., Lu, Q. M., Nakamura, R., Huang, C., Du, A. M., Guo, F., et al. (2016). Coalescence of magnetic flux ropes in the ion diffusion region of magnetic reconnection. *Nature Physics*, 12(3), 263–267. <https://doi.org/10.1038/nphys3578>
- Wang, R. S., Yu, X. C., Wang, Y. M., Lu, Q. M., & Lu, S. (2023). Observation of the Hall magnetic reconnection as close as 56 solar radii from the Sun. *The Astrophysical Journal*, 947(2), 78. <https://doi.org/10.3847/1538-4357/acbdf6>
- Wang, S. M., Wang, R. S., Lu, Q. M., Burch, J. L., Cohen, I. J., Jaynes, A. N., & Ergun, R. E. (2023). Electron acceleration by interaction of two filamentary currents within a magnetopause magnetic flux rope. *Geophysical Research Letters*, 50(11). <https://doi.org/10.1029/2023gl103203>
- Wang, S. M., Wang, R. S., Lu, Q. M., Fu, H. S., & Wang, S. (2020). Direct evidence of secondary reconnection inside filamentary currents of magnetic flux ropes during magnetic reconnection. *Nature Communications*, 11(1), 3964. <https://doi.org/10.1038/s41467-020-17803-3>
- Wang, S. M., Wang, R. S., Lu, Q. M., Russell, C. T., Ergun, R. E., & Wang, S. (2021). Large-scale parallel electric field collocated in an extended electron diffusion region during the magnetosheath magnetic reconnection. *Geophysical Research Letters*, 48(23). <https://doi.org/10.1029/2021gl094879>

- Wang, S. M., Wang, R. S., Yao, S. T., Lu, Q. M., Russell, C. T., & Wang, S. (2019). Anisotropic electron distributions and whistler waves in a series of the flux transfer events at the magnetopause. *Journal of Geophysical Research: Space Physics*, *124*(3), 1753–1769. <https://doi.org/10.1029/2018ja026417>
- Wang, Y. L., Elphic, R. C., Lavraud, B., Taylor, M. G. G. T., Birn, J., Raeder, J., et al. (2005). Initial results of high-latitude magnetopause and low-latitude flank flux transfer events from 3 years of Cluster observations. *Journal of Geophysical Research*, *110*(A11). <https://doi.org/10.1029/2005ja011150>
- Wilder, F. D., Ergun, R. E., Burch, J. L., Ahmadi, N., Eriksson, S., Phan, T. D., et al. (2018). The role of the parallel electric field in electron-scale dissipation at reconnecting currents in the magnetosheath. *Journal of Geophysical Research: Space Physics*, *123*(8), 6533–6547. <https://doi.org/10.1029/2018ja025529>
- Yao, S. T., Hamrin, M., Shi, Q. Q., Yao, Z. H., Degeling, A. W., Zong, Q., et al. (2020). Propagating and dynamic properties of magnetic dips in the dayside magnetosheath: MMS observations. *Journal of Geophysical Research: Space Physics*, *125*(6). <https://doi.org/10.1029/2019ja026736>
- Yao, S. T., Shi, Q. Q., Liu, J., Yao, Z. H., Guo, R. L., Ahmadi, N., et al. (2018). Electron dynamics in magnetosheath mirror-mode structures. *Journal of Geophysical Research: Space Physics*, *123*(7), 5561–5570. <https://doi.org/10.1029/2018ja025607>
- Yao, S. T., Wang, X. G., Shi, Q. Q., Pitkänen, T., Hamrin, M., Yao, Z. H., et al. (2017). Observations of kinetic-size magnetic holes in the magnetosheath. *Journal of Geophysical Research: Space Physics*, *122*(2), 1990–2000. <https://doi.org/10.1002/2016ja023858>
- Zenitani, S., Hesse, M., Klimas, A., & Kuznetsova, M. (2011). New measure of the dissipation region in collisionless magnetic reconnection. *Physical Review Letters*, *106*(19), 195003. <https://doi.org/10.1103/physrevlett.106.195003>
- Zhang, H., Kivelson, M. G., Angelopoulos, V., Khurana, K. K., Pu, Z. Y., Walker, R. J., et al. (2012). Generation and properties of in vivo flux transfer events. *Journal of Geophysical Research*, *117*(A5). <https://doi.org/10.1029/2011ja017166>
- Zhong, Z. H., Tang, R., Zhou, M., Deng, X., Pang, Y., Paterson, W., et al. (2018). Evidence for secondary flux rope generated by the electron Kelvin-Helmholtz instability in a magnetic reconnection diffusion region. *Physical Review Letters*, *120*(7), 075101. <https://doi.org/10.1103/physrevlett.120.075101>
- Zhong, Z. H., Zhou, M., Tang, R. X., Deng, X. H., Khotyaintsev, Y. V., Giles, B. L., et al. (2020). Extension of the electron diffusion region in a guide field magnetic reconnection at magnetopause. *The Astrophysical Journal Letters*, *892*(1), L5. <https://doi.org/10.3847/2041-8213/ab7b7c>
- Zhou, M., Berchem, J., Walker, R., El-Alaoui, M., Deng, X., Cazzola, E., et al. (2017). Coalescence of macroscopic flux ropes at the subsolar magnetopause: Magnetospheric Multiscale observations. *Physical Review Letters*, *119*(5), 055101. <https://doi.org/10.1103/physrevlett.119.055101>